metals

Article

Picolinoyl N4-Phenylthiosemicarbazide-Modified ZnAl and ZnAlCe Layered Double Hydroxide Conversion Films on Hot-Dip Galvanized Steel for Enhancing Corrosion Protection in Saline Solution

Thu Thuy Pham [1], Anh Son Nguyen [2], Chien Thang Pham [3], Hong Nhung Nguyen [3], Maurice Gonon [1], Lisa Dangreau [4], Xavier Noirfalise [4], Thuy Duong Nguyen [2], Thi Xuan Hang To [2] and Marie-Georges Olivier [1,4,*]

[1] Materials Science Department, Université de Mons, Place du Parc 20, 7000 Mons, Belgium; thuthuy.pham@umons.ac.be (T.T.P.); maurice.gonon@umons.ac.be (M.G.)
[2] Institute of Materials Science, Vietnam Academy of Science and Technology, 18 Hoang Quoc Viet, Nghia Do, Hanoi 10000, Vietnam; nason@ims.vast.ac.vn (A.S.N.); ntduong@ims.vast.ac.vn (T.D.N.); ttxhang@ims.vast.vn (T.X.H.T.)
[3] Faculty of Chemistry, VNU University of Science, Vietnam National University, Hanoi, 19 Le Thanh Tong, Hanoi 12016, Vietnam; phamchienthang@hus.edu.vn (C.T.P.); nguyenhongnhung_t65@hus.edu.vn (H.N.N.)
[4] Materia Nova, Parc Initialis, 7000 Mons, Belgium; lisa.dangreau@materianova.be (L.D.); xavier.noirfalise@materianova.be (X.N.)
* Correspondence: marjorie.olivier@umons.ac.be; Tel.: +32-65-37-44-31

Abstract

ZnAl and ZnAlCe layered double hydroxide (LDH) conversion layers modified with picolinoyl N4-phenylthiosemicarbazide (**HL**) are fabricated on hot-dip galvanized steel (HDG) to improve corrosion protection. X-ray diffraction (XRD) confirms that **HL** molecules are not intercalated within the LDH interlayers, whereas Fourier transform infrared spectroscopy (FT-IR), X-ray photoelectron spectroscopy (XPS), and energy-dispersive X-ray spectroscopy (EDS) analyses reveal their surface adsorption. Moreover, scanning electron microscopy (FE-SEM) observations reveal that **HL** modification induces changes in surface morphology. After 168 h in 0.1 M NaCl, the LDH structure remains intact, and N and S signals are still detected, confirming the persistence of both the LDH layer and adsorbed **HL** molecules under corrosive conditions. During 168 h immersion in NaCl, electrochemical measurements indicate that the modified LDH layers exhibit higher corrosion resistance than the unmodified ones, with the ZnAlCe LDH/**HL** coating providing the most effective protection.

Keywords: layered double hydroxide; hot-dip galvanized steel; acyl thiosemicarbazide; corrosion protection

Academic Editor: Eric Hug

Received: 19 November 2025
Revised: 8 January 2026
Accepted: 12 January 2026
Published: 19 January 2026

1. Introduction

Zinc is widely employed as a sacrificial coating for the corrosion protection of steel across numerous sectors [1]. Among the available deposition techniques, hot-dip galvanizing (HDG) remains particularly attractive due to its low cost, operational simplicity, and ability to produce robust, adherent zinc coatings [2]. Upon exposure to the environment, the galvanized surface develops a corrosion product film, comprising basic zinc oxides, zinc hydroxides, and zinc carbonates, that contributes significantly to its protective performance [2,3]. Nevertheless, the corrosion protection afforded by HDG coatings is not

always uniform, and localized degradation can occur, particularly in chloride-rich environments [3]. To enhance the durability of galvanized steel under such aggressive conditions, conversion layers are routinely applied. Chromate conversion coatings were widely used because of their excellent corrosion resistance and intrinsic self-healing capability [4,5]. However, traditional chromate treatments typically rely on hexavalent chromium (Cr^{6+}), whose high toxicity and carcinogenicity have prompted stringent regulatory restrictions and a pressing need for safer alternatives [5]. In response, considerable studies have focused on the development of environmentally benign conversion coatings. Promising candidates include molybdate-based systems, rare-earth-metal-containing coatings, sol–gel coatings and layered double hydroxide (LDH) layers, all of which have demonstrated potential to improve corrosion resistance while eliminating the hazards associated with Cr^{6+}-containing processes [6–8].

LDHs are a group of layered inorganic compounds composed of positively charged brucite-like layers and charge-compensating interlayer anions [9,10]. Owing to their unique lamellar architecture and high anion-exchange capacity, LDHs have garnered significant interest in the field of metal corrosion protection [10,11]. When incorporated into primer coatings, LDHs can function as nanocontainers to immobilize corrosion inhibitors, enabling a controlled release of protective species while simultaneously trapping aggressive ions [11]. This dual functionality imparts both barrier protection and self-healing capability to the coating system. Moreover, LDH layers can be directly fabricated on metallic substrates, either as standalone protective layers or as pretreatment layers that enhance the adhesion and performance of subsequent topcoats [9,12–14].

A variety of corrosion inhibitors have been successfully incorporated into LDH layers on Mg and Al alloy substrates to enhance active protection. Y. Wang et al. fabricated ZnAlCe-LDH layers on 6061 Al alloy by electrodeposition and demonstrated higher corrosion protection compared with ZnAl-LDH layers [15]. The improved performance was attributed to Ce^{3+} incorporation, which facilitated the formation of compact, thick layers with stronger barrier properties, efficient chloride entrapment, and redox-driven self-healing at localized defects. Neves et al. demonstrated that ZnAl-LDH layers on AA2024 alloy, modified with mercaptobenzothiazole (MBT), provided not only barrier protection but also self-healing capability through the release and adsorption of inhibitors at defect sites [16]. Likewise, LiAl-LDH intercalated with vanillin L-aspartic acid anions produced a compact and uniform layer on A6N01-T5 Al alloy, exhibiting superior ion-exchange capacity and significantly improved corrosion resistance compared to the unmodified LDH layer [17]. X. Wang et al. prepared MgAl-CO_3 LDH layers on AZ31 Mg alloy using the hydrothermal method, followed by functionalization with 8-hydroxyquinoline (8HQ) [18]. They found that MgAl-LDH layers loaded with 8HQ provided localized protection by forming stable Mg-HQ complexes at defect sites, thereby suppressing pitting. Yao et al. fabricated MgAlLa-LDH films intercalated with sodium benzoate on AZ31 Mg alloy substrate, which provided corrosion protection through inhibitor release and barrier effects [19]. When transformed into slippery liquid-infused porous surfaces, the coatings exhibited outstanding durability, with long-lasting corrosion resistance as well as self-cleaning and self-healing capabilities.

Recent studies have demonstrated feasible methods for the direct growth of LDH layers on zinc and its alloys substrates. Zheludkevich et al. demonstrated that a ZnAl-NO_3 LDH layer can be directly synthesized on zinc substrate via a one-step hydrothermal process in $Al(NO_3)_3/NaNO_3$ solution at 90 °C for 20 h [20–23]. The resulting nitrate-intercalated LDH layer acted as an effective precursor for anion exchange, with in situ synchrotron studies revealing reaction rates following the sequence $Cl^- > SO_4^{2-} > VO_x^{y-}$ [22]. Furthermore, EIS and SVET confirmed that both nitrate- and vanadate-intercalated LDH layers

significantly enhanced the corrosion resistance of zinc in 0.05 M NaCl solution, with a ZnAl-V_2O_7 LDH sample providing superior protection compared to a ZnAl-NO_3 LDH sample [23]. This can be explained by the partial release of vanadate species, which form protective surface films that inhibit both anodic zinc dissolution and cathodic oxygen reduction. Xu et al. synthesized a ZnAl-NO_3 LDH layer on galvanized steel using a two-step electrochemical method at room temperature, where anodic dissolution of zinc generates Zn^{2+} near the substrate and subsequent cathodic deposition promotes LDH layer growth [13]. These layers were further functionalized by incorporating corrosion inhibitors such as 8-HQ, which endowed the coatings with dual protection by acting as both a physical barrier and a reservoir for inhibitor release in chloride-containing environments. Amanian et al. modified ZnAl-CO_3 LDH layer with benzotriazole (BTA) via ion-exchange [6]. This improved the corrosion resistance of galvanized steel, increasing impedance up to four times compared with the unmodified layer. The released BTA not only adsorbed onto the metal surface but also formed stable Zn-BTA complexes at defect sites, enabling a self-healing effect. In our previous work, ZnAlCe-CO_3 HT layers were synthesized on HDG substrates under different precursor pH conditions [24]. It was demonstrated that Ce^{3+} and Ce^{4+} species can be released from the LDH lattice and reprecipitate as insoluble cerium oxides/hydroxides at cathodic sites, thereby sealing local defects, suppressing oxygen reduction, and providing self-healing functionality.

Thiosemicarbazide (TSC) derivatives, owing to their effective inhibition performance at low concentrations and comparatively lower hazardous character, offer a promising alternative to conventional toxic corrosion inhibitors and may support the transition toward more environmentally responsible protection strategies [25–29]. Their effectiveness is attributed to the presence of multiple donor atoms, including nitrogen, sulfur, and oxygen, as well as π-electrons from conjugated bonds, which facilitate strong adsorption on metal surfaces. Upon adsorption, these molecules can form stable metal–inhibitor complexes that block active sites, suppress anodic metal dissolution, and retard cathodic reactions, thereby reducing overall corrosion rates. Chauhan et al. evaluated TSC-functionalized chitosan for mild steel in 1 M HCl and achieved inhibition efficiencies above 90% at relatively low concentrations, with adsorption obeying the Langmuir isotherm and supported by DFT and molecular dynamics simulations [28]. Singh et al. reported that TSC acted as an effective corrosion inhibitor for copper in chloride media, with efficiency improving with concentration [29]. The protective effect was attributed to the formation of Cu(I)–TSC surface complexes, which further oxidized into stable Cu(II) species, thereby reducing anodic dissolution and enhancing resistance against chloride attack. In our recent study, acyl thiosemicarbazide compounds, including picolinoyl N4-phenylthiosemicarbazide (**HL**), were demonstrated to be highly effective mixed-type corrosion inhibitors for zinc in neutral saline environments, providing inhibition efficiencies exceeding 97% at 1.0×10^{-3} M [30]. Electrochemical analyses indicated that these compounds simultaneously suppressed anodic and cathodic reactions, while DFT calculations and XPS results confirmed their strong adsorption capability and the formation of stable Zn-N and Zn-S coordination bonds, consistent with the experimentally observed corrosion protection behavior.

Despite its proven efficiency, the combination of TSC with LDH coatings has not yet been reported. Given the ion-exchange capacity and active protection offered by LDHs, the incorporation of TSC into their structure could integrate the barrier properties of LDHs with the strong inhibition capability of TSC. On this basis, the present study aims to develop and evaluate TSC-modified LDH layers on HDG substrates as a novel strategy for enhanced corrosion protection. Specifically, ZnAl and ZnAlCe LDH layers are functionalized with picolinoyl N4-phenylthiosemicarbazide (**HL**), and their structural characteristics as well

as corrosion resistance are systematically investigated. The modified LDHs are characterized before and after immersion in saline solution using FT-IR, XRD, SEM/EDS, and XPS analyses. In addition, electrochemical techniques, including polarization curves and electrochemical impedance spectroscopy (EIS), are employed to evaluate the inhibition efficiency of the LDH samples during 168 h of exposure to saline solution.

2. Materials and Methods

2.1. Materials

The HDG plates (wt%: Zn 92.1, Al 1.2, C 3.9, O 2.8) are supplied by ArcelorMittal (Ghent, Belgium) [24]. Before LDH layer growth, the substrates are degreased with acetone and ethanol, followed by immersion in a commercial alkaline cleaning solution (Gardoclean®, Frankfurt, Germany) [31].

Analytical-grade reagents, including $Al(NO_3)_3 \cdot 9H_2O$ (Darmstadt, Germany), $Ce(NO_3)_3 \cdot 6H_2O$ (Darmstadt, Germany), $Zn(NO_3)_2 \cdot 7H_2O$ (Darmstadt, Germany), NaCl (Darmstadt, Germany), and NaOH (Darmstadt, Germany), were used in all experiments. Picolinoyl N4-phenylthiosemicarbazide (**HL**) is prepared in accordance with a standard procedure [32,33].

2.2. LDHs Conversion Layer Preparation

ZnAl LDH and ZnAlCe LDH conversion layers are prepared at pH 12, as reported earlier [24,34]. Briefly, HDG substrates are immersed in a mixed solution of $Zn(NO_3)_2$, $Al(NO_3)_3$, NaOH, and $Ce(NO_3)_3$ for ZnAlCe LDH synthesis at room temperature under stirring for 6 h, followed by 16 h without stirring (Scheme 1). The specimens are then removed, rinsed with DI water, and dried. Then, the specimens are immersed in a 1 mM **HL** solution (the pH is adjusted to 12 using 1 M NaOH) for 2 h at room temperature (Scheme 1). After removal, they are rinsed with DI water and dried with compressed air. The modified layers are denoted ZnAl LDH/**HL** and ZnAlCe LDH/**HL**.

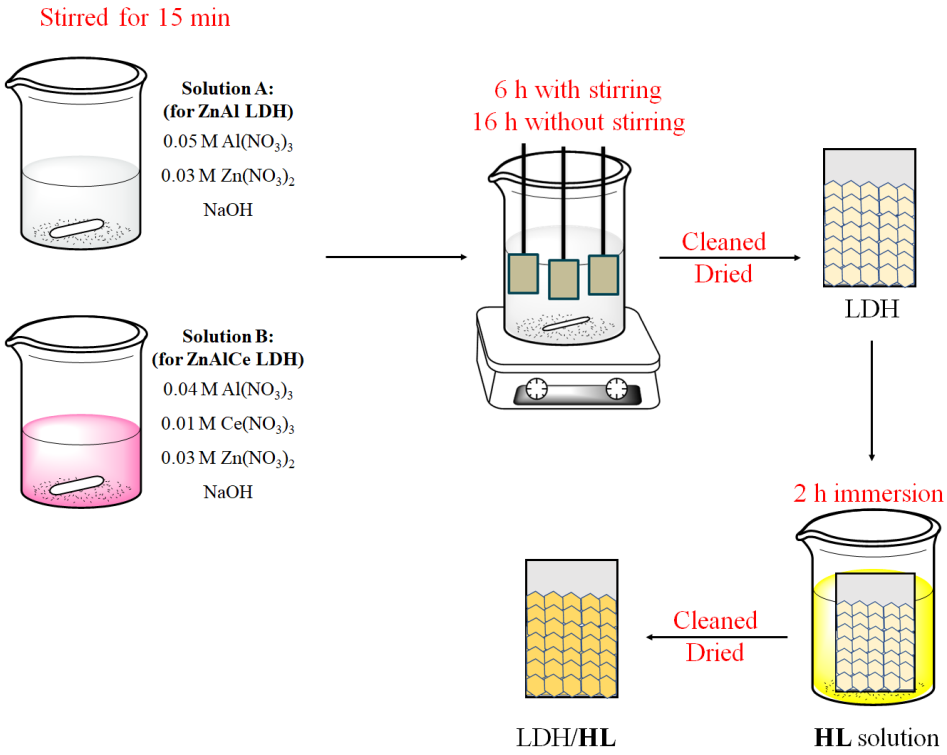

Scheme 1. Diagram for the preparation of ZnAl LDH/**HL** and ZnAlCe LDH/**HL** layers.

2.3. Characterization

The functional groups on the surface of the modified LDH layers are analyzed by FTIR (Nexus 670, Nicolet, Waltham, MA, USA). The phase composition of LDH layers is determined by XRD (Bruker D5000, Billerica, MA, USA) using CoKα radiation (λ = 0.1789 nm) with an Fe filter at a scan speed of 1° min^{-1}. The surface composition of the LDH layers is characterized by XPS (PHI VERSAPROBE 5000, Chigasaki, Japan) with Al Kα radiation (1486.6 eV). Measurements are conducted using a 200 μm beam diameter at 50 W. Atomic compositions were obtained from peak areas after applying Shirley baseline correction. FE-SEM (Hitachi SU8020, Tokyo, Japan) coupled with EDS (Thermo Scientific Noran System 7, Waltham, MA, USA) is used to analyze the microstructure and compositions of the LDH layers.

2.4. Electrochemical Tests

The corrosion behavior of LDH layers in 0.1 M NaCl solution is evaluated over 168 h immersion using a Parstat Model 2273 (Oak Ridge, TN, USA) controlled by Powersuite® 2.3 software. A conventional three-electrode cell is employed, with an Ag/AgCl (sat. KCl) reference electrode, a spiral-shaped platinum counter electrode, and the LDH layers (1 cm^2 exposed area) serving as the working electrode. Before EIS and polarization curve measurements, all samples are allowed to stabilize at open-circuit potential (OCP) for 15 min. EIS measurements are carried out within the frequency range of 100 kHz to 10 mHz with a sinusoidal perturbation of ±5 mV (peak-to-peak). Polarization curves are recorded over potential ranges of +0.03 to −0.40 V and −0.03 to +0.40 V versus OCP (V vs. Ag/AgCl) at 0.2 mV s^{-1}. The electrochemical tests are conducted inside a Faraday cage to suppress external electromagnetic disturbances and ensure stable, noise-free impedance responses. All electrochemical tests are performed at least in duplicate.

3. Results

3.1. Characterization of LDH Conversion Layers

3.1.1. FT-IR Results

Figure 1 shows the FT-IR spectra of **HL** compound, unmodified and modified LDH layers. As observed for unmodified LHD [24,34], the FT-IR spectra of the LDH/**HL** samples display a characteristic broad band at around 3410 cm^{-1}, which correspond to O–H vibrations of water molecules and hydroxyl groups. The bands observed at wavenumbers below 800 cm^{-1} are attributed to lattice vibrations of M–O, O–M–O, and M–O–M units (M = Zn, Al, or Ce) within the LDH framework [35]. Consistent with the unmodified LDH samples [24,34], the LDH/**HL** materials exhibit a distinct absorption band at around 1355 cm^{-1}, which corresponds to the stretching vibrations of intercalated CO_3^{2-} ions. However, the FT-IR spectra of **HL**-modified LDH samples exhibit characteristic absorption bands in the range of 1560–1400 cm^{-1}, representing the stretching vibration of C–C bonds from the aromatic ring structure of **HL** [30,33]. Additionally, characteristic **HL** peaks around 1230 cm^{-1}, likely due to interactions between the valence vibrations of C=S and C–N/C=N bonds, appear in the FT-IR spectrum [30,33]. The **HL** characteristic peaks in the ZnAl LDH/**HL** and ZnAlCe LDH/**HL** spectra confirm the presence of **HL** molecules in the modified specimen.

3.1.2. XRD Results

Figure 2 shows XRD patterns of modified LDH layers with **HL** solution prepared on HDG before and after 168 h immersion in 0.1 M NaCl. The characteristic diffraction reflections (003), (006), and (012) of LDH layers appeared at approximately 13.7°, 27.5°, and 40.7°, respectively, indicating the existence of carbonate-intercalated LDH structure, consistent

with the FT-IR absorption band observed near 1355 cm^{-1} (Figure 2a) [31]. This phenomenon can be explained by the fact that, in alkaline media, dissolved CO_2 readily reacts with hydroxide ions to generate CO_3^{2-} species, which are preferentially and rapidly incorporated into the LDH interlayer galleries, thereby stabilizing the carbonate-intercalated LDH structure [35]. Compared to the unmodified LDH samples [24,34], ZnAl LDH/**HL** and ZnAlCe LDH/**HL** layers do not show any new peak related to d(003), suggesting that **HL** molecules are not intercalated within the LDH interlayer galleries.

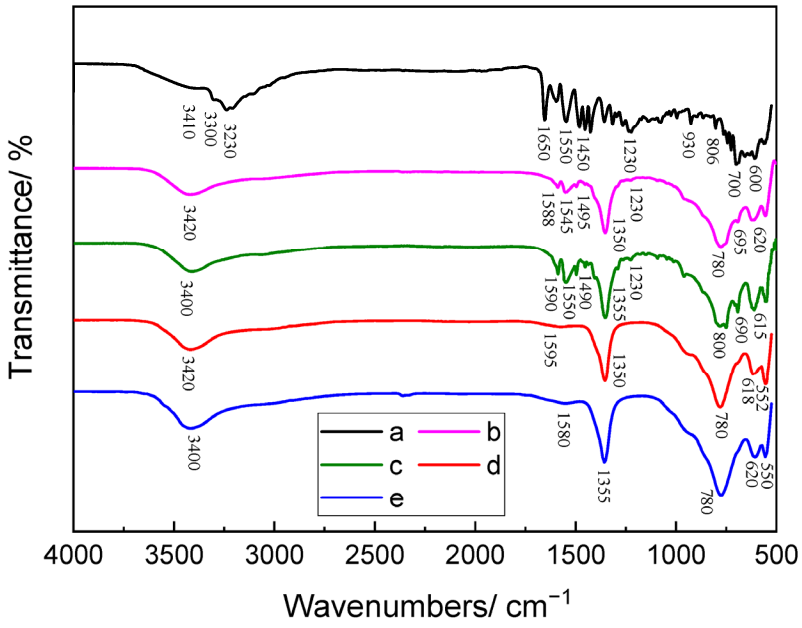

Figure 1. FT-IR spectra of (a) **HL**, (b) ZnAl LDH/**HL**, (c) ZnAlCe LDH/**HL**, (d) ZnAl and (e) ZnAlCe LDH samples (The FT-IR spectra of ZnAl LDH and ZnAlCe LDH samples are adapted from Refs. [24,34]).

After immersion in NaCl solution, the characteristic diffraction peaks corresponding to carbonate-intercalated LDH structures remain visible in the XRD patterns (Figure 2b). The characteristic peaks of simonkolleite are observed only on the HDG substrate, which are not detected on modified LDH layers, suggesting that the LDH layers limit simonkolleite formation. Similar to the unmodified LDH samples [24,34], additional peaks attributed to ZnO crystalline phases are also detected, indicating the formation of ZnO on LDH layers as a corrosion product [31].

3.1.3. XPS Results

To further examine the surface properties of modified LDH layers, XPS analyses are performed before and after immersion for 168 h in 0.1 M NaCl, as shown in Figures 3–5. Similar to the unmodified LDH layers, the XPS spectra of the **HL**-modified samples display characteristic peaks assigned to O 1s, Zn 2p, Al 2p, and Ce 3d (for ZnAlCe LDH/**HL**), with no significant changes in peak positions observed after modification with **HL** (Figure 3) [24,34]. Notably, after treatment with the **HL** solution, new signals appear at approximately 400 eV and 163 eV, attributed to the presence of N 1s and S 2p, respectively (Figure 3). These results suggest the presence of **HL** molecules on the surface of the LDH layers.

In comparison with the unmodified LDH layers [24,34], the O 1s, Zn $2p_{3/2}$, Al 2p, and Ce 3d spectra show no significant changes (Figures 4 and 5). In the O 1s spectrum (Figures 4c and 5c), the three peaks at about 533.1, 531.4, and 529.6 eV can be assigned to carboxyl group, hydroxide group, and lattice O^{2-} bonds of LDH [9,36]. The Zn $2p_{3/2}$

spectra exhibit a primary peak at around 1022.4 eV, which is attributed to Zn–OH bond (Figures 4e and 5e) [36]. The Al 2p spectra show two peaks at 75.5 and 74.4 eV, which are related to Al–O and Al–OH bonds [24]. The Ce 3d spectrum for ZnAlCe LDH/**HL** exhibits peaks in the ranges of about 918.1–898.1 eV and 894.9–880.1 eV, which are assigned to the Ce $3d_{3/2}$ and Ce $3d_{5/2}$, respectively (Figure 5g) [24,37]. The v, v_3, and u multiples correspond to the binding energies characteristic of Ce^{3+}, while the v_1, v_2, u_1, u_2, and u_3 multiples are indicative of Ce^{4+}, confirming that the coexistence of Ce^{3+} and Ce^{4+} oxidation states in the modified LDH layers [24].

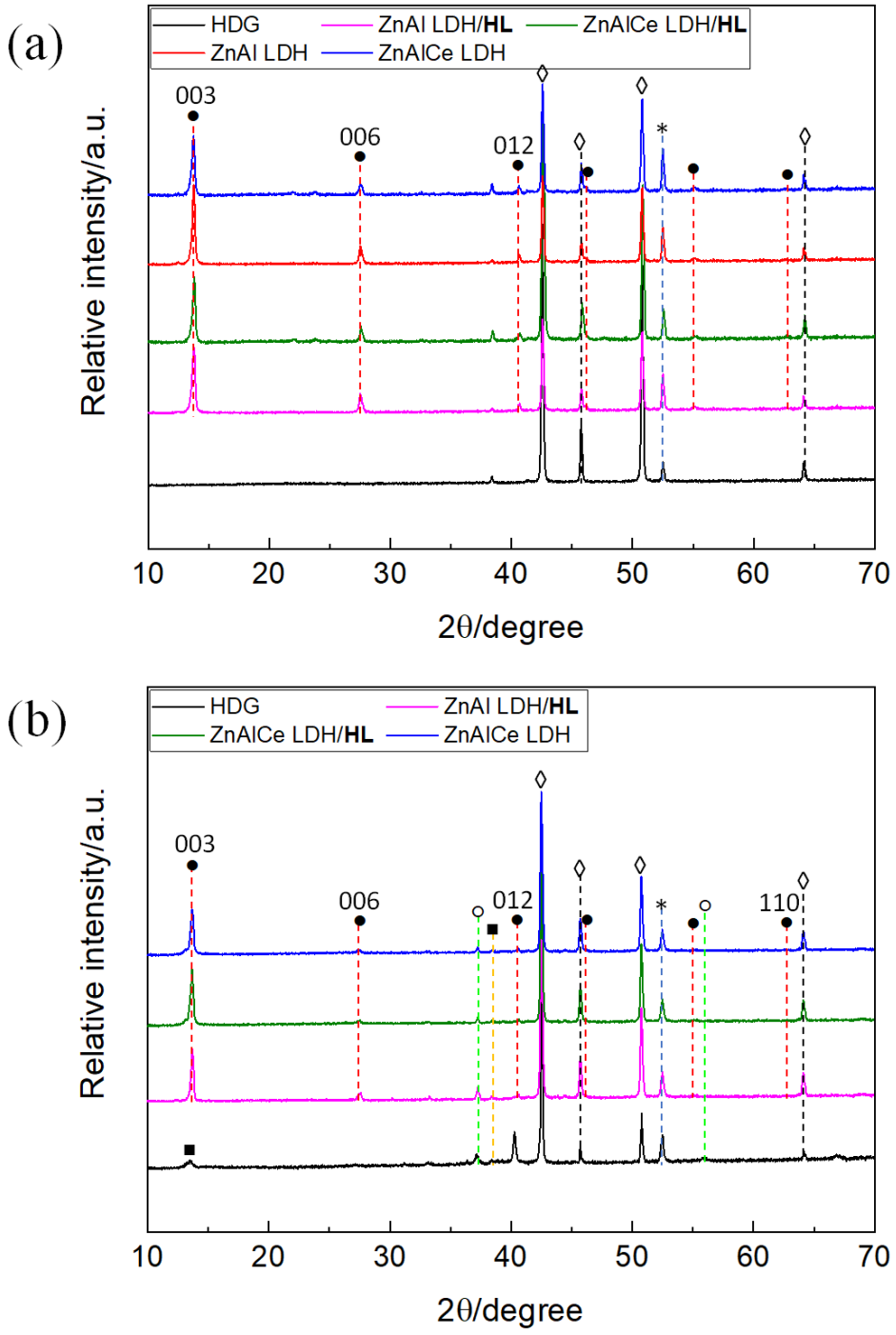

Figure 2. XRD patterns of HDG, ZnAl LDH/**HL**, ZnAlCe LDH/**HL**, ZnAl LDH and ZnAlCe LDH: (**a**) before and (**b**) after 168 h immersion in NaCl solution. ●: LDH; ◊: zinc; *: iron; ○: zinc oxide; and ■: simonkolleite (the XRD results of ZnAl LDH and ZnAlCe LDH samples are adapted from Refs. [24,34]).

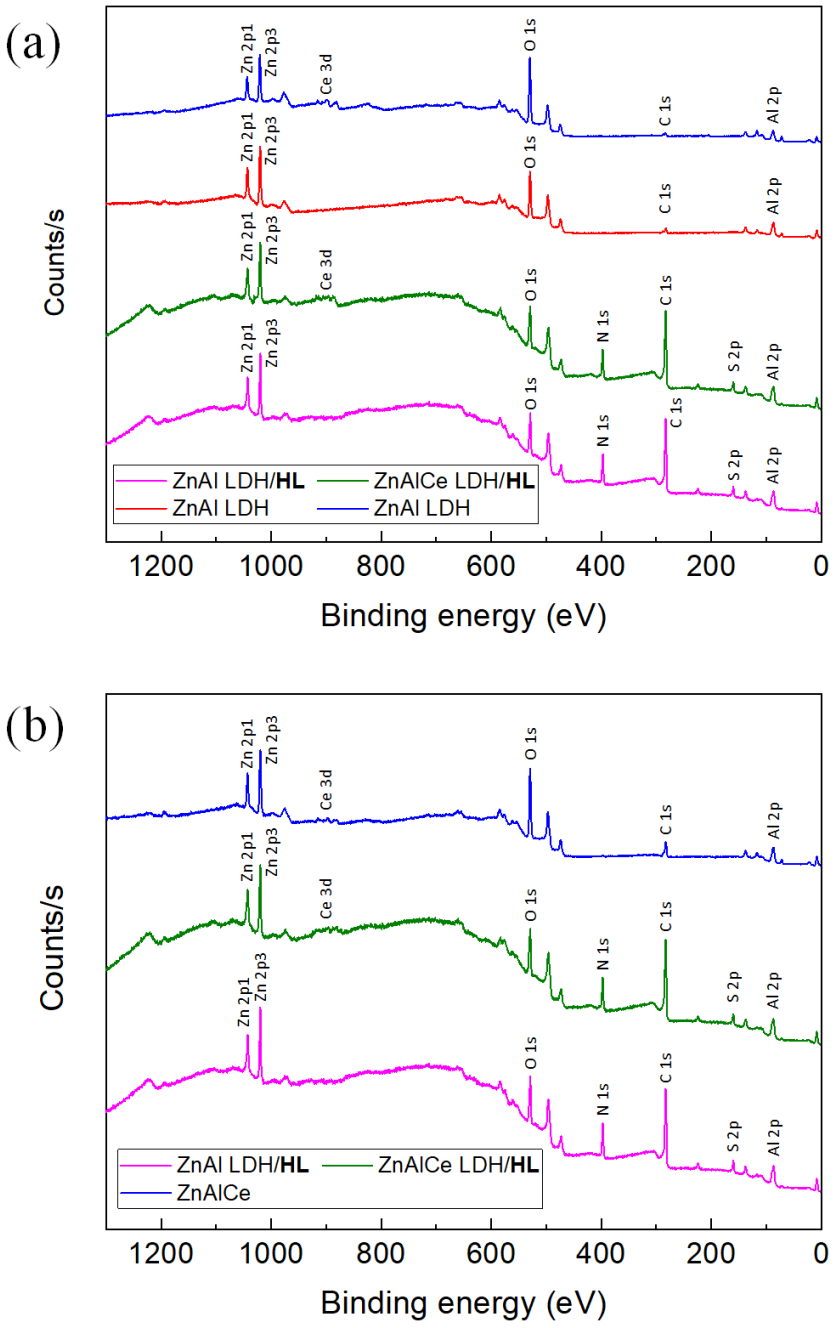

Figure 3. XPS spectra survey of ZnAl LDH/**HL**, ZnAlCe LDH/**HL**, ZnAl LDH and ZnAlCe LDH samples (**a**) before and (**b**) after 168 h immersion in NaCl solution (the XPS results of ZnAl LDH and ZnAlCe LDH samples are adapted from Refs. [24,34]).

Compared with the unmodified LDH layers, the C 1s spectrum of the modified samples exhibits notable differences. The spectrum can be resolved into four distinct peaks centered at approximately 288.0, 287.5, 286.5, and 284.5 eV, which correspond to the bonds between C and N, O, S atoms from **HL** molecules, and C–O/C=O bonds associated with CO_3^{2-} anions (Figures 4a and 5a) [30,38–40]. The N 1s spectrum shows two peaks at 399.8 eV and 398.4 eV, which are assigned to the N–H and N–C bonds, respectively, within the **HL** molecules (Figures 4b and 5b) [38,39]. Additionally, the presence of a shoulder peak at a binding energy higher than that of the N–H bond suggests increased nitrogen oxidation states, indicating chemical adsorption of **HL** onto the LDH layer through nitrogen atoms [41]. The high-resolution S 2p spectra display pronounced signals with noticeable asymmetry, indicating the presence of sulfur atoms in two distinct chemical states. The

peaks at 164.0 eV (S $2p_{1/2}$) and 162.5 eV (S $2p_{3/2}$) are attributed to the C=S bonds in the **HL** molecules (Figures 4d and 5d) [42,43]. Moreover, a shoulder peak near 161.5 eV suggests a chemical interaction between sulfur atoms and the LDH surface [43]. These features confirm the incorporation of **HL** molecules within the LDH layers.

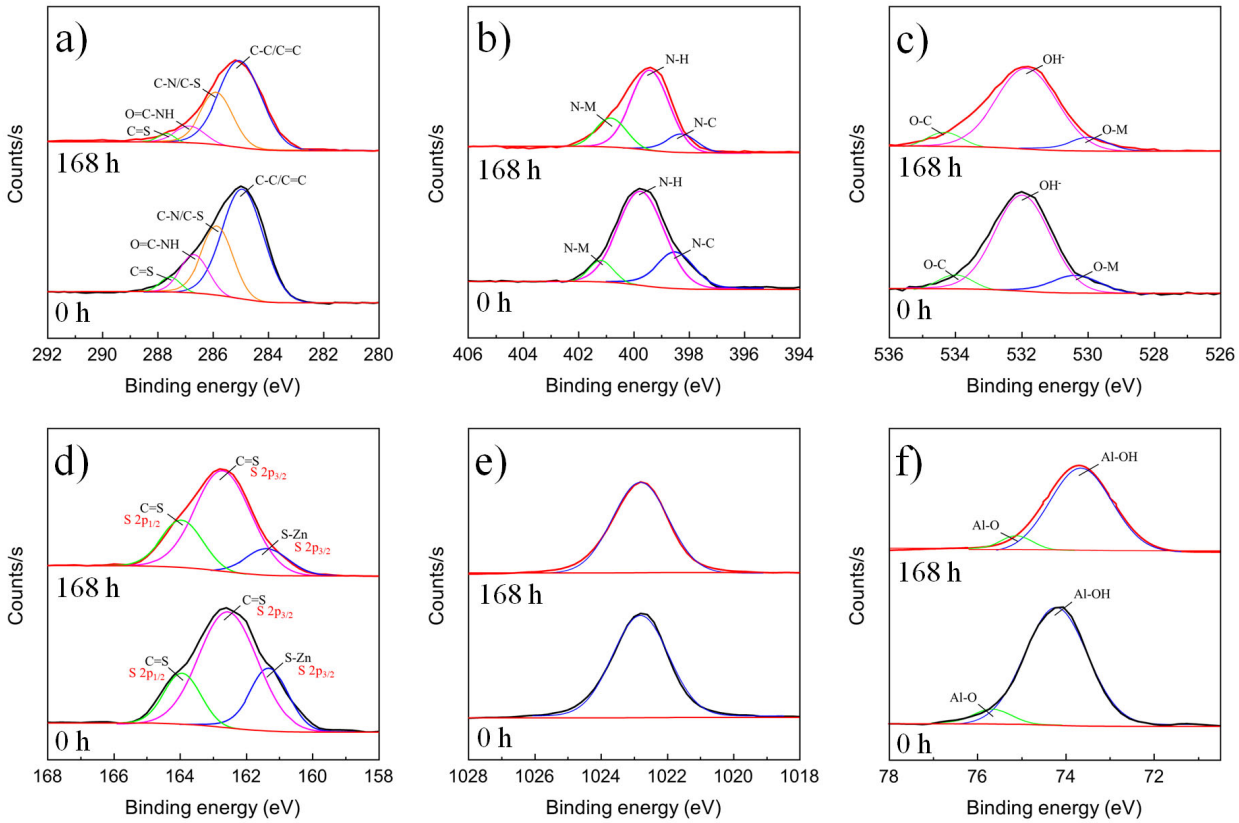

Figure 4. High resolution XPS spectra of ZnAl LDH/**HL** before and after immersion in NaCl: (**a**) C 1s, (**b**) N 1s, (**c**) O 1s, (**d**) S 2p, (**e**) Zn 2p3, and (**f**) Al 2p.

After 168 h of immersion, the characteristic peaks of the LDH layers (O 1s, Zn 2p, Al 2p, and Ce 3d) remain observable, confirming their structural stability (Figure 3b). Additionally, the observed C 1s, N 1s, and S 2p peaks also confirm the persistence of **HL** molecules within the LDH layers (Figure 3b). It is noteworthy that the intensity of these peaks slightly decreases after NaCl exposure, suggesting partial degradation (Figures 4 and 5). Similar to the unmodified LDH layers [24], the Ce 3d spectrum of the ZnAlCe LDH/**HL** sample exhibited multiple peaks corresponding to Ce $3d_{3/2}$ and Ce $3d_{5/2}$, indicating the presence of both of Ce^{3+} and Ce^{4+} oxidation states after NaCl immersion (Figure 5g).

3.1.4. FE-SEM/EDS Results

FE-SEM and EDS are employed to characterize the morphology and elemental composition of the modified LDH samples. The FE-SEM results (Figure 6a,c) show that the deposited layers are non-uniform. As seen in Figure 6(a1), the ZnAl LDH/**HL** phase formed away from the HDG substrate consists of hexagonal plate-like crystallites, typical of LDH structures. These crystallites are relatively similar in shape to those observed for the unmodified ZnAl LDH layer [34]. The LDH layer directly formed on the HDG surface (Figure 6(a2)) exhibits a rose petal-like nanostructure, where the hexagonal nanosheets are tightly packed and interconnected. The nanosheets in the ZnAlCe LDH/**HL** layer are randomly oriented and unevenly distributed over the surface (Figure 6c). Compared to ZnAlCe LDH [24], this random orientation confirms that the **HL** modification did not significantly alter the intrinsic growth behavior of the LDH nanosheets. EDS analysis (Table 1)

indicates that, apart from the principal elements such as Zn, Al, O, and Ce in the ZnAlCe LDH/**HL** sample, the modified LDH layers also contain detectable amounts of N and S atoms. The presence of N and S confirms the successful adsorption of **HL** molecules on the LDH surface, consistent with the XPS findings. Moreover, the relatively low concentrations of N and S (below 1 wt%) indicate that **HL** molecules may be mainly located on the outer surface of the LDH layers rather than intercalated within the interlayer galleries.

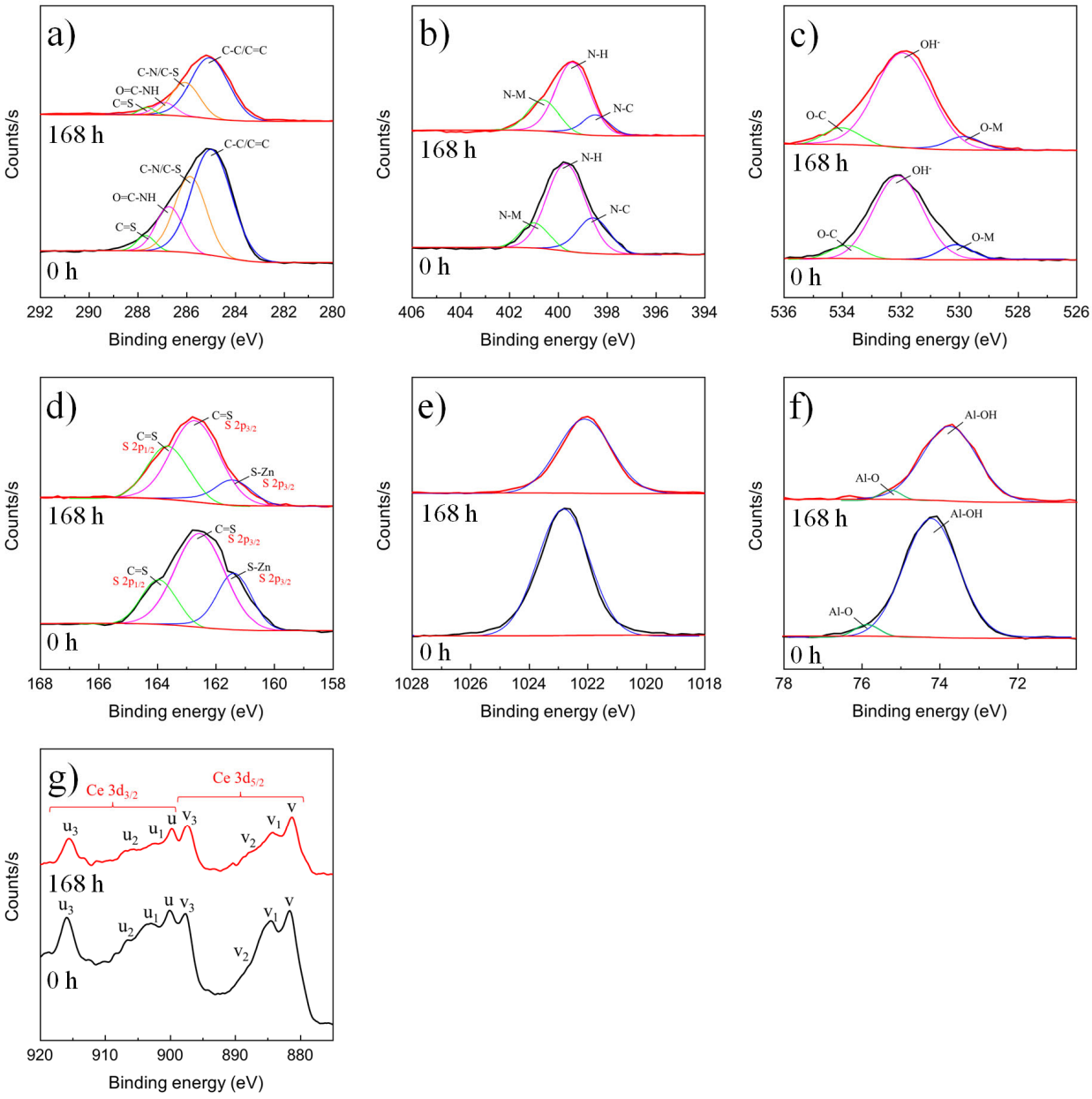

Figure 5. High-resolution XPS spectra of ZnAlCe LDH/**HL** before and after immersion in NaCl: (**a**) C 1s, (**b**) N 1s, (**c**) O 1s, (**d**) S 2p, (**e**) Zn 2p3, (**f**) Al 2p, and (**g**) Ce 3d.

After 168 h of immersion, the SEM micrographs (Figure 6b,d) show that both ZnAl LDH/**HL** and ZnAlCe LDH/**HL** layers remain relatively intact, although slight morphological changes are observed. For the ZnAl LDH/**HL** sample, partial dissolution and thinning of the nanosheets occur. This indicates that prolonged exposure to chloride solution gradually weakens the structural integrity of the LDH layer. In contrast, the ZnAlCe LDH/**HL** coating exhibits a more compact and continuous morphology, with fewer visible defects. The nanosheets appear more densely stacked, suggesting that the presence of Ce species

contributes to improved structural stability and corrosion resistance. The presence of N and S atoms remains detectable, suggesting that a portion of **HL** remains anchored to the LDH surface, thereby contributing to the sustained corrosion inhibition of the modified layers. All samples showed a rise in O content following exposure to the NaCl solution, indicating the formation of oxygen-containing corrosion products such as ZnO, which aligns with the XRD findings (Table 1). The continued detection of N and S atoms suggests that residual **HL** molecules are still attached to the LDH surface.

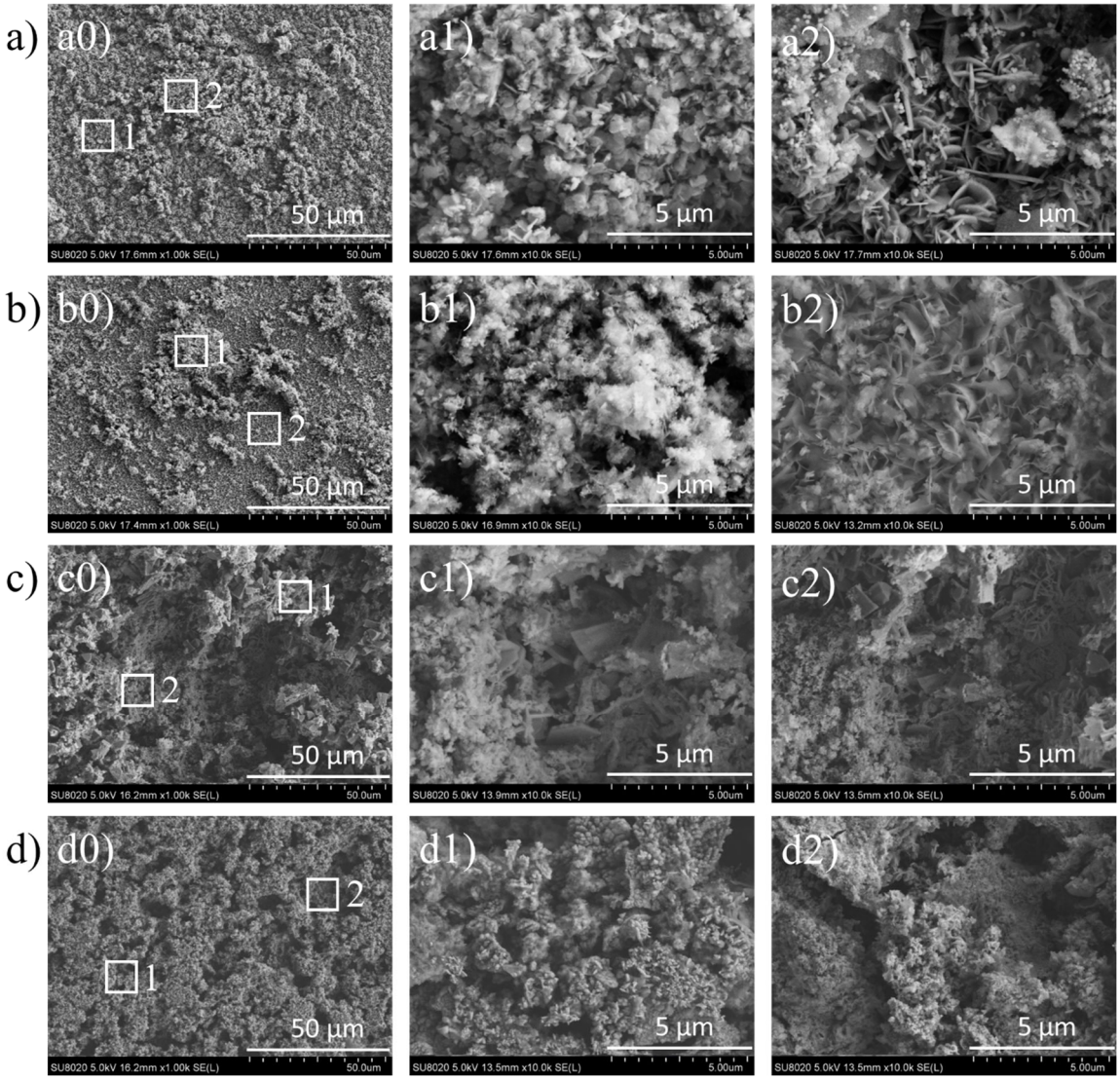

Figure 6. SEM micrographs of (**a**) and (**b**) ZnAl LDH/**HL** before and after NaCl immersion, (**c**) and (**d**) ZnAlCe LDH/**HL** before and after NaCl immersion.

3.2. Corrosion Protection of LDH Layers

For such conversion layers, continuous immersion testing is more appropriate, as it allows direct monitoring of corrosion processes and inhibitor activity using electrochemical techniques (OCP, polarization curves, and EIS). In contrast, salt spray testing is highly accelerated and may cause premature degradation of thin conversion layers, making it less suitable for mechanistic evaluation. Therefore, immersion testing is intentionally selected to reliably assess the corrosion behavior and protection mechanism of the LDH conversion coatings studied in this work.

Table 1. EDS test results of ZnAl LDH and ZnAlCe LDH layers.

Sample	Element Content (wt%)						
	O	**Al**	**Zn**	**Ce**	**Cl**	**N**	**S**
Before immersion in NaCl							
ZnAl LDH/**HL**	32.0	7.4	56.6	-	-	0.9	0.4
ZnAlCe LDH/**HL**	35.8	9.6	44.1	6.2	-	1.0	0.4
After 168 h of immersion in NaCl							
ZnAl LDH/**HL**	39.7	5.9	50.2	-	0.3	0.7	0.3
ZnAlCe LDH/**HL**	40.4	7.7	41.2	5.5	0.2	0.8	0.4

3.2.1. OCP Monitoring and Polarization Curves

The OCP evolution of HDG substrates, with and without modified LDH layers by **HL**, is monitored during 168 h immersion in NaCl solution (Figure 7). The LDH-coated samples exhibit more positive OCP values than the bare substrate. As shown in Figure 7, the OCP values of the HDG substrate range from −1.03 V to −1.07 V, whereas those of the LDH-coated samples range from −0.97 V to −1.01 V during the 168 h immersion. Moreover, the modification leads to a positive shift in OCP for both LDH samples, with the modified ZnAl LDH and modified ZnAlCe LDH showing higher OCP values than their corresponding unmodified LDH layers [24,34]. This improvement is likely linked to the gradual release of **HL** molecules from the LDH and their adsorption onto anodic regions, thereby limiting the anodic dissolution process. Among the coatings, ZnAlCe LDH/**HL** exhibit the highest OCP values, which can be ascribed to the discharge of cerium ions from the LDH [24]. Acting as cathodic inhibitors, the cerium cations adsorb onto cathodic sites, enhancing corrosion protection of the metal.

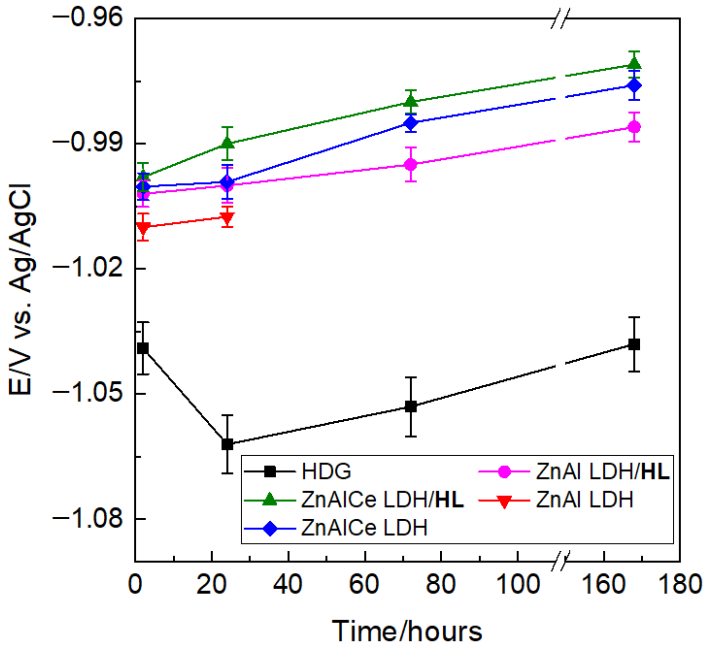

Figure 7. OCP variations with immersion time for HDG and LDH layers (the OCP results of ZnAl LDH and ZnAlCe LDH samples are adapted from Refs. [24,34]).

The inhibition behavior of the LDH layers is assessed through polarization curves after 24 h and 168 h of immersion (Figure 8). To provide a meaningful comparison, the polarization curves of HDG substrates immersed in NaCl solution supplemented with 1 mM **HL** are analyzed alongside those of the **HL**-modified LDH coatings. The **HL**-

modified LDH samples exhibit lower current densities compared to the bare HDG substrate, indicating a significant reduction in the corrosion rate. Importantly, the current densities of the **HL**-modified LDH samples are also consistently lower than those measured for the corresponding unmodified LDH layers [24,34]. Furthermore, the current densities of the **HL**-modified LDH coatings are noticeably lower than those of the HDG substrate immersed in the **HL**-containing electrolyte, demonstrating that the LDH layers enhance the inhibitory performance beyond that provided by the **HL** molecules alone. This improvement can be attributed to the ability of LDH to act as both a reservoir and a controlled-release platform for **HL**, ensuring sustained delivery of inhibitor species and providing an additional physical barrier that restricts the transport of corrosive ions [6,23]. Notably, the current density of the ZnAlCe LDH/**HL** layer is lower than that of the ZnAl LDH/**HL** layer during immersion. In the case of ZnAlCe LDH/**HL**, a combined effect between **HL** anions and cerium cations enhances the corrosion protection provided by the LDH layer.

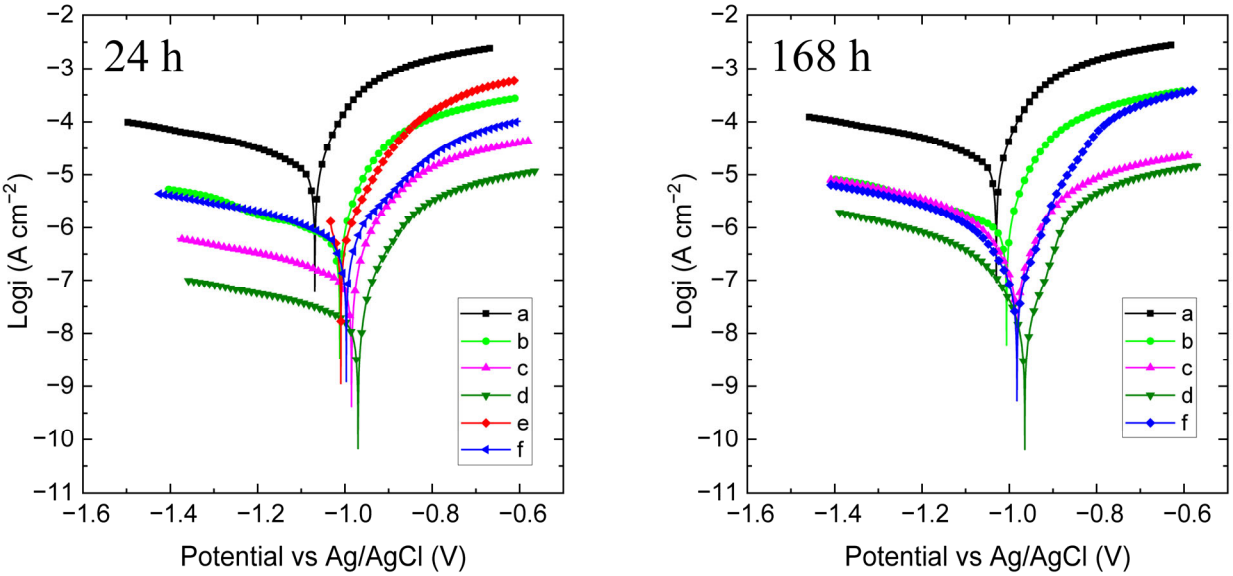

Figure 8. Polarization curve after 24 h and 168 h of immersion: (a) HDG substrate in 0.1 M NaCl, (b) HDG substrate in 0.1 M NaCl + 1 mM **HL**, (c) ZnAl LDH/**HL** sample in 0.1 M NaCl, (d) ZnAlCe LDH/**HL** sample in 0.1 M NaCl, (e) ZnAl LDH sample in 0.1 M NaCl and (f) ZnAlCe LDH sample in 0.1 M NaCl (the results of ZnAl LDH and ZnAlCe LDH samples are adapted from Refs. [24,34]).

3.2.2. Electrochemical Investigations

EIS is employed to assess the influence of modified LDH layers by **HL** on the corrosion resistance of the HDG substrate (Figure 9 and Table 2). In comparison with the bare HDG substrate (reported in [3]), the presence of LDH layers markedly improves corrosion protection. As summarized in Table 2, the impedance modulus at low frequency (0.01 Hz) for the LDH-coated samples is approximately several times greater than that of bare HDG [3]. Furthermore, the modified LDH layers exhibit higher impedance values at low frequencies than their unmodified ones in previous studies, reflecting the additional protective contribution of the incorporated **HL** inhibitor (Figure 10 and Table 2) [24,34]. In agreement with the polarization measurements, the EIS results demonstrate that the concurrent presence of **HL** anions and cerium cations in LDH layer yields superior corrosion protection (Table 2).

To quantitatively evaluate the corrosion behavior and elucidate the protective mechanism of the LDH layers, the EIS spectra are analyzed by fitting to an appropriate electrical circuit (EC). Similar to the pure LDH layers [24,34], three distinct time constants are observed in the impedance responses of all modified LDH-coated samples; therefore, the EC shown in Figure 9e is employed for fitting the EIS data. The R_{f1} and R_{f2} values of

the modified LDH layers, which are associated with the barrier properties of the oxide layer and the LDH layer, increase over the immersion period. Moreover, these values are slightly higher than those of the unmodified LDH layers (Table 2) [24,34]. Notably, after 168 h of immersion, the R_{f1} and R_{f2} values of the ZnAlCe LDH/**HL** layer are 1890 and 6402 $\Omega \cdot cm^2$, respectively, representing markedly higher values than those obtained for the ZnAl LDH/**HL** layer (Table 2). In parallel, the Q_{f1} (5.42×10^{-5} $\Omega^{-1} \cdot s^n \cdot cm^{-2}$) and Q_{f2} (6.21×10^{-5} $\Omega^{-1} \cdot s^n \cdot cm^{-2}$) obtained for the ZnAl LDH/**HL** coating are significantly reduced in the ZnAlCe LDH/**HL** system ($Q_{f1} = 4.02 \times 10^{-6}$ $\Omega^{-1} \cdot s^n \cdot cm^{-2}$ and $Q_{f2} = 3.01 \times 10^{-5}$ $\Omega^{-1} \cdot s^n \cdot cm^{-2}$). The pronounced increase in R_f together with the marked reduction in Q_f values indicate a substantial enhancement in the corrosion protection afforded by the ZnAlCe LDH/**HL** coating. It should be noted that the decrease in Q_f, combined with the n values shifting towards 0.5, reflects a more complex barrier layer where diffusion-controlled processes within the LDH matrix contribute to the overall protection, underscoring the combined beneficial contributions of **HL** anions and cerium cations [18,24].

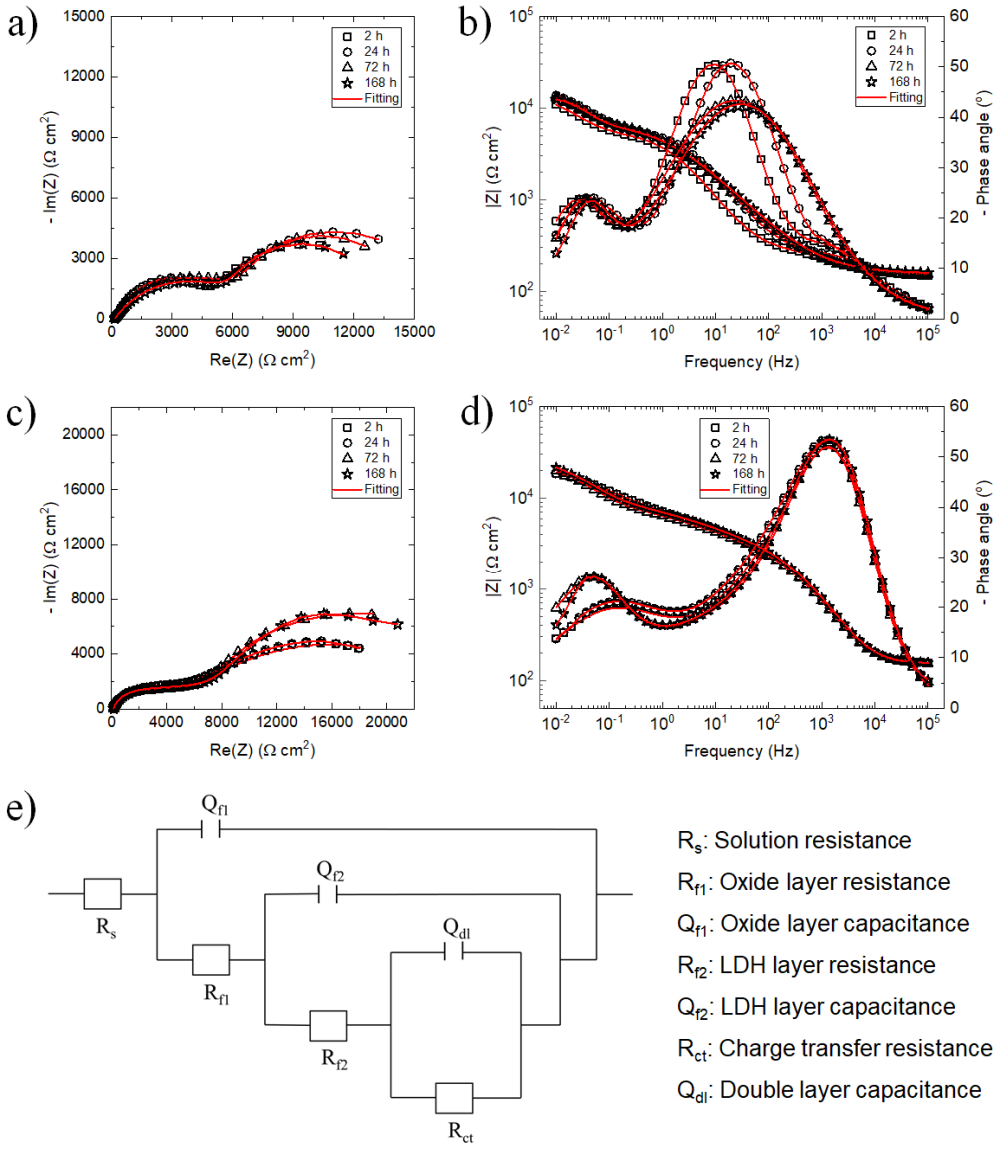

Figure 9. EIS spectra of (**a**,**b**) ZnAl LDH/**HL** layer, (**c**,**d**) ZnAlCe LDH/**HL** layer during 168 h immersion in NaCl, and (**e**) EC for fitting of EIS data.

Table 2. The circuit fitted parameters of LDH layers (The results of ZnAl LDH and ZnAlCe LDH samples are adapted from Refs. [24,34]).

Samples	Time (h)	Q_{f1} ($\Omega^{-1}\cdot s^{n}\cdot cm^{-2}$)	n_{f1}	R_{f1} ($\Omega\cdot cm^{2}$)	Q_{f2} ($\Omega^{-1}\cdot s^{n}\cdot cm^{-2}$)	n_{f2}	R_{f2} ($\Omega\cdot cm^{2}$)	Q_{dl} ($\Omega^{-1}\cdot s^{n}\cdot cm^{-2}$)	n	R_{ct} ($\Omega\cdot cm^{2}$)	$\lvert Z \rvert_{10mHz}$ ($\Omega\cdot cm^{2}$)
ZnAl LDH/**HL**	2	1.61×10^{-5}	0.72	188	2.15×10^{-5}	0.80	5166	1.95×10^{-4}	0.81	7430	10,921
	24	1.89×10^{-5}	0.71	268	3.25×10^{-5}	0.82	5846	2.85×10^{-4}	0.83	10,360	13,788
	72	4.38×10^{-5}	0.64	319	5.74×10^{-5}	0.73	6041	4.57×10^{-4}	0.80	9840	13,039
	168	5.42×10^{-5}	0.62	332	6.21×10^{-5}	0.71	6025	5.85×10^{-4}	0.80	7810	12,434
ZnAlCe LDH/**HL**	2	4.25×10^{-6}	0.88	1771	1.45×10^{-5}	0.54	5312	1.15×10^{-4}	0.84	20,670	18,448
	24	4.29×10^{-6}	0.89	1802	1.49×10^{-5}	0.55	6001	1.18×10^{-4}	0.85	21,260	18,533
	72	4.30×10^{-6}	0.90	1889	2.05×10^{-5}	0.55	6325	1.20×10^{-4}	0.89	23,210	20,097
	168	4.02×10^{-6}	0.90	1890	3.01×10^{-5}	0.55	6402	1.22×10^{-4}	0.89	26,010	21,663
ZnAl LDH	2	1.89×10^{-5}	0.7	182	2.34×10^{-5}	0.85	4803	1.08×10^{-3}	0.75	6071	9927
	24	3.01×10^{-5}	0.74	489	7.24×10^{-5}	0.75	4087	1.32×10^{-3}	0.83	8777	8615
ZnAlCe LDH	2	5.17×10^{-6}	0.88	1684	1.65×10^{-5}	0.55	4926	2.89×10^{-4}	0.73	11,640	13,049
	24	5.71×10^{-6}	0.88	1609	2.02×10^{-5}	0.52	5033	1.74×10^{-4}	0.71	10,920	12,664
	72	5.94×10^{-6}	0.88	1630	1.84×10^{-5}	0.53	5152	1.27×10^{-4}	0.82	18,700	18,282
	168	3.30×10^{-6}	0.90	1709	4.45×10^{-5}	0.55	5370	1.37×10^{-4}	0.90	25,340	21,078

https://doi.org/10.3390/met16010115

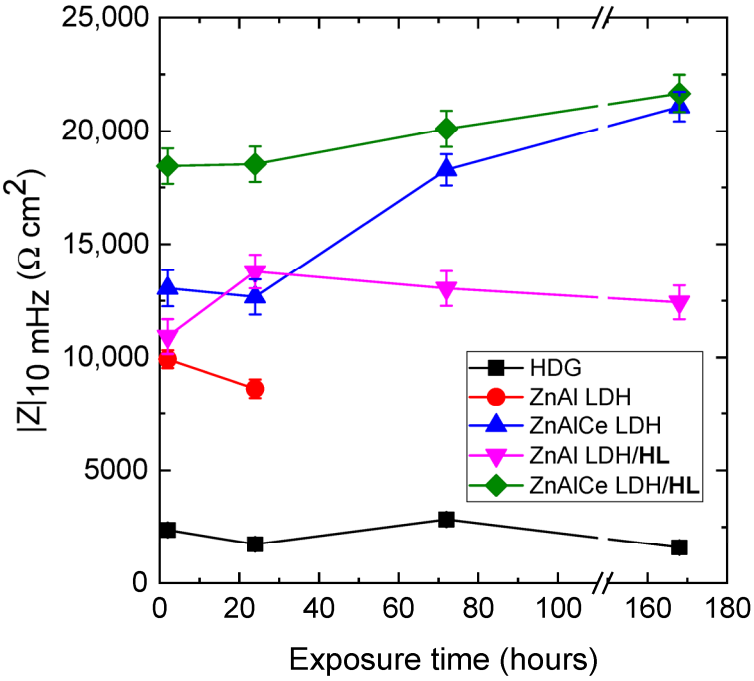

Figure 10. The values $|Z|_{10mHz}$ of HDG substrate and LDH layers during exposure time (the values $|Z|_{10mHz}$ of ZnAl LDH and ZnAlCe LDH samples are adapted from Refs. [24,34]).

The ZnAlCe LDH/**HL** sample demonstrates higher resistance R_{ct} and lower CPE_{dl} parameter, indicating better protective properties than that of the ZnAl LDH/**HL** sample during 168 h (Table 2). For the ZnAl LDH/**HL** layer, the R_{ct} values increased from 7430 Ω·cm^2 at 2 h to 10,360 Ω·cm^2 at 24 h, followed by a decrease to 7810 Ω·cm^2 after 168 h (Table 2). The initial increase in R_{ct} values can be ascribed to the release and adsorption of **HL** anions from the LDH layer onto the metal interface, forming a barrier that impedes electron transfer [10,44]. However, the subsequent decrease in R_{ct} values with prolonged immersion may be related to a gradual depletion or leaching of **HL** inhibitor, together with electrolyte penetration through coating defects, leading to the breakdown of the protective layer and a reduction in corrosion protection efficiency [10,44]. The ZnAlCe LDH/**HL** layer exhibits R_{ct} values of 20,670 and 21,260 Ω·cm^2 after 2 h and 24 h, respectively, which are nearly double those measured for the unmodified ZnAlCe LDH [24]. The R_{ct} of the ZnAlCe LDH/**HL** layer increases to 26,010 Ω·cm^2 after 168 h, but this value only slightly exceeds that of the unmodified HT layer. Similar to the ZnAl LDH/**HL** sample, these results suggest that the improved inhibition at the beginning of immersion may be attributed to the contribution of **HL** molecules. Nevertheless, the long-term protective performance may be more related to the presence of cerium, which promotes the precipitation of cerium oxides/hydroxides at cathodic regions and enhances the structural integrity of the LDH matrix [24,45,46].

4. Discussion

XRD analysis of modified LDH samples reveals no shift or appearance of new (003) and (006) reflections, indicating that **HL** molecules are not intercalated within the LDH layers. However, the XPS spectra display distinct N 1s and S 2p signals, confirming the presence of **HL** at the outer surface of LDH layers. These results suggest that **HL** molecules are mainly adsorbed onto the surface rather than incorporated into the LDH crystal lattice. In this work, the modified LDH-coated samples display significantly improved corrosion resistance relative to the HDG substrates. Importantly, the LDH layers developed in this study show higher protective performance than previously reported unmodified LDH

ones [24,34]. The corrosion protection of LDH layers is attributed to the physical barrier effect, which prevents direct exposure of the HDG substrate to chloride ions from the corrosive medium [23,31].

At the early stages of immersion in NaCl, the beneficial role of **HL** becomes particularly evident. Compared with the unmodified LDH sample, the **HL**-modified layers exhibited more positive OCP values, which can be attributed to the initial release of **HL** molecules from the LDH surface, which rapidly adsorb onto anodic sites of the metal substrate and suppress the anodic dissolution process (Figures 7 and 8). In parallel, EIS measurements reveal that the impedance modulus at low frequencies is significantly higher for the **HL**-modified layers than for their unmodified ones, further confirming that the enhanced barrier properties are provided by the presence of **HL** (Figures 9 and 10) [24,34]. However, after prolonged immersion, the protective effect of the ZnAl LDH/**HL** layer gradually decreases. This decline can be correlated with the leaching of **HL** molecules from the LDH surface, which diminishes the reservoir of active inhibitor available for re-adsorption at anodic sites. Concurrently, electrolyte ingress through coating defects compromises the structural integrity of the protective layer and reduces its long-term corrosion resistance.

In contrast, the corrosion protection of the ZnAlCe LDH/**HL** layer increases progressively with immersion time, highlighting the beneficial role of cerium incorporation (Figure 8). Our previous study indicates that the presence of cerium species contributes to a more compact and defect-tolerant coating, where cerium compounds can partially block nanoscale pores and microdefects within the LDH structure, thereby hindering chloride ion diffusion toward the substrate [24]. Considering the solubility products of $Zn(OH)_2$ (1.2×10^{-17}), $Al(OH)_3$ (1.3×10^{-33}), $Ce(OH)_3$ (1.6×10^{-20}), and $Ce(OH)_4$ (2.0×10^{-48}) in aqueous solution at 10–20 °C, it is evident that Ce^{3+}/Ce^{4+} and Al^{3+} ions tend to precipitate as hydroxides more readily than Zn^{2+} [24]. As a result, when localized coating damage occurs, cerium hydroxides can deposit within the defective regions and on the exposed HDG substrate surface, sealing the active sites and mitigating localized corrosion. The precipitation of cerium cations can be described by the following reactions, Equations (1)–(4) [45,46]. The transformation of cerium hydroxides into their oxide counterparts can proceed through the reactions outlined in Equations (5) and (6), leading to the formation of stable CeO_2 phases within the LDH layer [24,45]. The incorporation of **HL** together with cerium enhances the corrosion resistance of the LDH layer. Specifically, **HL** improves the initial protective performance, whereas cerium species maintain long-term stability by precipitating as insoluble hydroxide/oxide phases. These deposits effectively block active sites and damaged regions, thereby providing a sustained self-healing capability to LDH layer.

$$Ce^{3+} + 3\,OH^- \rightarrow Ce(OH)_3 \quad (1)$$

$$Ce^{4+} + 4\,OH^- \rightarrow Ce(OH)_4 \quad (2)$$

$$4\,Ce^{3+} + 4\,OH^- + O_2 + 2\,H_2O \rightarrow 4\,Ce(OH)_2{}^{2+} \quad (3)$$

$$Ce(OH)_2{}^{2+} + 2\,OH^- \rightarrow Ce(OH)_4 \quad (4)$$

$$2\,Ce(OH)_3 \rightarrow Ce_2O_3 + 3\,H_2O \quad (5)$$

$$Ce(OH)_4 \rightarrow CeO_2 + 2\,H_2O \quad (6)$$

5. Conclusions

The structural analyses collectively demonstrate that **HL** interacts with the outer surface of ZnAl and ZnAlCe LDH layers rather than entering their interlayer galleries. The adsorption of **HL** on the LDH surface improves the compactness and integrity of the layers, thereby enhancing its corrosion-inhibiting performance. Among all layers, the

ZnAlCe LDH/**HL** sample exhibits the highest impedance values and the lowest corrosion current density. The incorporation of Ce plays a crucial complementary role: cerium species contribute to the densification and stabilization of the LDH structure and can precipitate as cerium oxides/hydroxides at cathodic regions, sealing defects and imparting long-term self-healing protection. The combined action of **HL** adsorption and Ce-based barrier formation provides an effective route for improving the corrosion protection of LDH layers on HDG substrate.

Author Contributions: T.T.P.: Writing—original draft, Validation, Methodology, Investigation. A.S.N.: Validation, Investigation. C.T.P.: Validation, Supervision, Methodology. H.N.N.: Validation, Investigation. M.G.: Validation, Investigation. L.D.: Validation, Investigation. X.N.: Validation, Investigation. T.D.N.: Validation, Investigation. T.X.H.T.: Validation, Supervision, Methodology. M.-G.O.: Writing—review & editing, Supervision, Funding acquisition, Conceptualization. All authors have read and agreed to the published version of the manuscript.

Funding: The authors would like to acknowledge the financial support provided by ARES Belgium through the Development Cooperation project between Vietnam and Belgium (PRD 2020–2025) and the ARES Postdoc program (2025–2026). Anh Son Nguyen is funded by the Ministry of Science and Technology (Vietnam) under grant number DTDLCN.61/22.

Data Availability Statement: The original contributions presented in this study are included in the article. Further inquiries can be directed to the corresponding author.

Acknowledgments: The authors thank ArcelorMittal for supplying the metallic substrate.

Conflicts of Interest: Authors Lisa Dangreau, Xavier Noirfalise and Marie-Georges Olivier were employed by the Materia Nova. The remaining authors declare that the research was conducted in the absence of any commercial or financial relationships that could be construed as a potential conflict of interest.

References

1. Peng, S.; Xie, S.-K.; Xiao, F.; Lu, J.-T. Corrosion behavior of spangle on a batch hot-dip galvanized Zn-0.05Al-0.2Sb coating in 3.5 wt.% NaCl solution. *Corros. Sci.* **2020**, *163*, 108237. [CrossRef]
2. Fedel, M.; Poelman, M.; Olivier, M.; Deflorian, F. Sebacic acid as corrosion inhibitor for hot-dip galvanized (HDG) steel in 0.1 M NaCl. *Surf. Interface Anal.* **2019**, *51*, 541–551. [CrossRef]
3. Pham, T.T.; Nguyen, T.D.; Nguyen, A.S.; Nguyen, T.T.; Gonon, M.; Belfiore, A.; Paint, Y.; To, T.X.H.; Olivier, M.G. Role of Al and Mg alloying elements on corrosion behavior of zinc alloy-coated steel substrates in 0.1 M NaCl solution. *Mater. Corros.* **2023**, *74*, 903–919. [CrossRef]
4. Zhang, X.; Sloof, W.; Hovestad, A.; Van Westing, E.; Terryn, H.; De Wit, J. Characterization of chromate conversion coatings on zinc using XPS and SKPFM. *Surf. Coat. Technol.* **2005**, *197*, 168–176. [CrossRef]
5. Tomachuk, C.R.; Elsner, C.I.; Di Sarli, A.R.; Ferraz, O.B. Morphology and corrosion resistance of Cr(III)-based conversion treatments for electrogalvanized steel. *J. Coat. Technol. Res.* **2009**, *7*, 493–502. [CrossRef]
6. Amanian, S.; Naderi, R.; Mahdavian, M. Benzotriazole modified Zn-Al layered double hydroxide conversion coating on galvanized steel for improved corrosion resistance. *J. Taiwan Inst. Chem. Eng.* **2023**, *150*, 105072. [CrossRef]
7. Agustín-Sáenz, C.; Martín-Ugarte, E.; Jorcin, J.B.; Imbuluzqueta, G.; Santa Coloma, P.; Izagirre-Etxeberria, U. Effect of organic precursor in hybrid sol–gel coatings for corrosion protection and the application on hot dip galvanised steel. *J. Sol-Gel Sci. Technol.* **2018**, *89*, 264–283. [CrossRef]
8. Gao, Z.; Zhang, D.; Li, X.; Jiang, S.; Zhang, Q. Current status, opportunities and challenges in chemical conversion coatings for zinc. *Colloids Surf. A Physicochem. Eng. Asp.* **2018**, *546*, 221–236. [CrossRef]
9. Guo, X.; Xiong, Z.; Ma, F.; Wu, Q.; Ying, L.; Wang, G. Long-term corrosion resistance of superhydrophobic Ce-Co-Al LDH composite coatings prepared on the surface of Al alloy. *Surf. Interfaces* **2025**, *56*, 105601. [CrossRef]
10. Cao, J.; Wu, Y.; Zhao, W. Review of Layered Double Hydroxide (LDH) Nanosheets in Corrosion Mitigation: Recent Developments, Challenges, and Prospects. *Materials* **2025**, *18*, 1190. [CrossRef]
11. Bai, W.; Zhang, X.; He, Z.; Qian, Y.; Jian, R.; Lin, Y.; Xu, Y. Intelligent anti-corrosion coating with multiple protections using active nanocontainers of Zn Al LDH equipped with ZIF-8 encapsulated environment-friendly corrosion inhibitors. *Prog. Org. Coat.* **2023**, *185*, 107940. [CrossRef]

12. Hao, M.; Tan, H.; Yang, W.; Yue, D.; Gao, L.; Wang, Z.; He, C. Effect of pH on long-term corrosion protection of Zn doped MgAl-LDHs coatings by in situ growth on 5052 aluminum alloy. *Surf. Interfaces* **2025**, *64*, 106349. [CrossRef]
13. Xu, T.; Yu, L.; Hu, J.-M. In-situ Zn-Al layered double hydroxide conversion coatings prepared on galvanized steels by a two-step electrochemical method. *Corros. Sci.* **2024**, *233*, 112057. [CrossRef]
14. Bouali, A.C.; Serdechnova, M.; Blawert, C.; Tedim, J.; Ferreira, M.G.S.; Zheludkevich, M.L. Layered double hydroxides (LDHs) as functional materials for the corrosion protection of aluminum alloys: A review. *Appl. Mater. Today* **2020**, *21*, 100857. [CrossRef]
15. Wang, Y.; Zhou, J.; Zhou, B.; Li, Y.; He, K.; Wei, Y. Electrodeposition preparation of ZnAlCe-LDH film for corrosion protection of 6061 Al alloy. *Mater. Lett.* **2024**, *359*, 135965. [CrossRef]
16. Neves, C.S.; Bastos, A.C.; Salak, A.N.; Starykevich, M.; Rocha, D.; Zheludkevich, M.L.; Cunha, A.; Almeida, A.; Tedim, J.; Ferreira, M.G.S. Layered Double Hydroxide Clusters as Precursors of Novel Multifunctional Layers: A Bottom-Up Approach. *Coatings* **2019**, *9*, 328. [CrossRef]
17. Lin, K.; Luo, X.; Pan, X.; Zhang, C.; Liu, Y. Enhanced corrosion resistance of LiAl-layered double hydroxide (LDH) coating modified with a Schiff base salt on aluminum alloy by one step in-situ synthesis at low temperature. *Appl. Surf. Sci.* **2019**, *463*, 1085–1096. [CrossRef]
18. Wang, X.; Li, L.; Xie, Z.-H.; Yu, G. Duplex coating combining layered double hydroxide and 8-quinolinol layers on Mg alloy for corrosion protection. *Electrochim. Acta* **2018**, *283*, 1845–1857. [CrossRef]
19. Yao, W.; Chen, Y.; Wu, L.; Jiang, B.; Pan, F. Preparation of slippery liquid-infused porous surface based on MgAlLa-layered double hydroxide for effective corrosion protection on AZ31 Mg alloy. *J. Taiwan Inst. Chem. Eng.* **2022**, *131*, 104176. [CrossRef]
20. Mikhailau, A.; Maltanava, H.; Poznyak, S.K.; Salak, A.N.; Zheludkevich, M.L.; Yasakau, K.A.; Ferreira, M.G.S. One-step synthesis and growth mechanism of nitrate intercalated ZnAl LDH conversion coatings on zinc. *Chem. Commun.* **2019**, *55*, 6878–6881. [CrossRef]
21. Bouali, A.C.; Iuzviuk, M.H.; Serdechnova, M.; Yasakau, K.A.; Wieland, D.C.F.; Dovzhenko, G.; Maltanava, H.; Zobkalo, I.A.; Ferreira, M.G.S.; Zheludkevich, M.L. Zn-Al LDH growth on AA2024 and zinc and their intercalation with chloride: Comparison of crystal structure and kinetics. *Appl. Surf. Sci.* **2020**, *501*, 144027. [CrossRef]
22. Iuzviuk, M.H.; Bouali, A.C.; Serdechnova, M.; Yasakau, K.A.; Wieland, D.C.F.; Dovzhenko, G.; Mikhailau, A.; Blawert, C.; Zobkalo, I.A.; Ferreira, M.G.S.; et al. In situ kinetics studies of Zn-Al LDH intercalation with corrosion related species. *Phys. Chem. Chem. Phys.* **2020**, *22*, 17574–17586. [CrossRef]
23. Yasakau, K.A.; Kuznetsova, A.; Maltanava, H.M.; Poznyak, S.K.; Ferreira, M.G.S.; Zheludkevich, M.L. Corrosion protection of zinc by LDH conversion coatings. *Corros. Sci.* **2024**, *229*, 111889. [CrossRef]
24. Pham, T.T.; Nguyen, T.D.; Nguyen, A.S.; Gonon, M.; Belfiore, A.; Paint, Y.; Hang To, T.X.; Olivier, M.-G. Influence of solution pH on the structure formation and protection properties of ZnAlCe hydrotalcites layers on hot-dip galvanized steel. *Surf. Coat. Technol.* **2023**, *472*, 129918. [CrossRef]
25. Badr, G.E. The role of some thiosemicarbazide derivatives as corrosion inhibitors for C-steel in acidic media. *Corros. Sci.* **2009**, *51*, 2529–2536. [CrossRef]
26. Mohan, P.; Kalaignan, G.P. 1, 4-Bis (2-nitrobenzylidene) thiosemicarbazide as Effective Corrosion Inhibitor for Mild Steel. *J. Mater. Sci. Technol.* **2013**, *29*, 1096–1100. [CrossRef]
27. Ramya, K.; Mohan, R.; Anupama, K.K.; Joseph, A. Electrochemical and theoretical studies on the synergistic interaction and corrosion inhibition of alkyl benzimidazoles and thiosemicarbazide pair on mild steel in hydrochloric acid. *Mater. Chem. Phys.* **2015**, *149–150*, 632–647. [CrossRef]
28. Chauhan, D.S.; Ansari, K.R.; Sorour, A.A.; Quraishi, M.A.; Lgaz, H.; Salghi, R. Thiosemicarbazide and thiocarbohydrazide functionalized chitosan as ecofriendly corrosion inhibitors for carbon steel in hydrochloric acid solution. *Int. J. Biol. Macromol.* **2018**, *107*, 1747–1757. [CrossRef] [PubMed]
29. Singh, M.M.; Rastogi, R.B.; Upadhyay, B.N.; Yadav, M. Thiosemicarbazide, phenyl isothiocyanate and their condensation product as corrosion inhibitors of copper in aqueous chloride solutions. *Mater. Chem. Phys.* **2003**, *80*, 283–293. [CrossRef]
30. Pham, T.T.; Pham, C.T.; Nguyen, H.N.; Nguyen, Q.K.; Nguyen, A.S.; Cornil, D.; Cornil, J.; Nguyen, T.D.; Belfiore, A.; To, T.X.H.; et al. Acyl thiosemicarbazides as novel inhibitors for zinc substrate in saline solution. *J. Mol. Struct.* **2026**, *1351*, 144342. [CrossRef]
31. Pham, T.T.; Nguyen, T.D.; Nguyen, A.S.; Paint, Y.; Gonon, M.; To, T.X.H.; Olivier, M.-G. A comparative study of the structure and corrosion resistance of ZnAl hydrotalcite conversion layers at different Al^{3+}/Zn^{2+} ratios on electrogalvanized steel. *Surf. Coat. Technol.* **2022**, *429*, 127948. [CrossRef]
32. El-Asmy, A.; Ibrahim, K.; Bekheit, M.; Mostafa, M. Synthesis and Structural Studies of Co (II), Ni (II), Cu (II), Zn (II) and Cd (II) Chelates Derived From Semicarbazide and Thiosemicarbazide Derivatives. *J. Synth. React. Inorg. Met.-Org. Chem.* **1985**, *15*, 287–300. [CrossRef]
33. Nguyen, H.H.; Pham, Q.T.; Phung, Q.M.; Le, C.D.; Pham, T.T.; Pham, T.N.O.; Pham, C.T. Syntheses, Structures, and Biological Activities of Pd(II) and Pt(II) Complexes with some 1-picolinoyl-4-substituted Thiosemicarbazides. *J. Mol. Struct.* **2022**, *1269*, 133871. [CrossRef]

34. Pham, T.T.; Nguyen, T.D.; Nguyen, A.S.; Gonon, M.; Noirfalise, X.; Paint, Y.; To, T.X.H.; Olivier, M.-G. Study of the formation and anti-corrosion properties of Zn Al hydrotalcite conversion films grown "in situ" on different zinc alloys coated steel. *Prog. Org. Coat.* **2022**, *173*, 107221. [CrossRef]
35. Hoshino, K.; Furuya, S.; Buchheit, R.G. Effect of Solution pH on Layered Double Hydroxide Formation on Electrogalvanized Steel Sheets. *J. Mater. Eng. Perform.* **2019**, *28*, 2237–2244. [CrossRef]
36. Shen, Y.; Zhang, D.; Zhang, Z.; Li, C.; Wu, W. High corrosion-resistant octanoic acid vapor-phase modified Ce-LDH surface film of aluminum alloy. *Colloids Surf. A Physicochem. Eng. Asp.* **2024**, *686*, 133370. [CrossRef]
37. Xuan, F.; Yan, Z.; Sun, Z. Efficient degradation of diuron using Fe-Ce-LDH/13X as novel heterogeneous electro-Fenton catalyst. *J. Electroanal. Chem.* **2022**, *910*, 116189. [CrossRef]
38. Wang, H.; He, T.; Quan, D.; Wang, T.; Li, C.; Shen, Y. Thiosemicarbazide-Linked Covalent Organic Framework: Preparation, Properties and Applications. *ChemistrySelect* **2021**, *6*, 11490–11495. [CrossRef]
39. Chen, Z.; Tang, B.; Niu, Y.; Chen, H.; Liu, Y.; Wang, A.; Bai, L. Synthesis of silica supported thiosemicarbazide for Cu(II) and Zn(II) adsorption from ethanol: A comparison with aqueous solution. *Fuel* **2021**, *286*, 119287. [CrossRef]
40. Qiu, Y.; Liu, Z.; Zhang, X.; Sun, A.; Liu, J. Interface engineering of double-layered nanosheets via cosynergistic modification by LDH interlayer carbonate anion and molybdate for accelerated industrial water splitting at high current density. *Appl. Surf. Sci.* **2022**, *598*, 153690. [CrossRef]
41. Goyal, P.; Menon, D.; Jain, P.; Prakash, P.; Misra, S.K. Linker mediated enhancement in reusability and regulation of Pb(II) removal mechanism of Cu-centered MOFs. *Sep. Purif. Technol.* **2023**, *318*, 123941. [CrossRef]
42. Kozlica, D.K.; Kokalj, A.; Milošev, I. Synergistic effect of 2-mercaptobenzimidazole and octylphosphonic acid as corrosion inhibitors for copper and aluminium—An electrochemical, XPS, FTIR and DFT study. *Corros. Sci.* **2021**, *182*, 109082. [CrossRef]
43. Deng, Q.; Jeschke, S.; Murdoch, B.J.; Hirth, S.; Eiden, P.; Gorges, J.N.; Keil, P.; Chen, X.-B.; Cole, I. In-depth insights of inhibitory behaviour of 2-amino-4-methylthiazole towards galvanised steel in neutral NaCl solution. *Corros. Sci.* **2022**, *199*, 110206. [CrossRef]
44. Zuo, J.D.; Peng, Z.C.; Dong, B.Q.; Wang, Y.S. In situ growth of corrosion resistant Mg-Fe layered double hydroxide film on Q235 steel. *J. Colloid Interface Sci.* **2022**, *610*, 202–212. [CrossRef]
45. Zahedi Asl, V.; Zhao, J.; Palizdar, Y.; Junaid Anjum, M. Influence of pH value and Zn/Ce cations ratio on the microstructures and corrosion resistance of LDH coating on AZ31. *Corros. Commun.* **2022**, *5*, 73–86. [CrossRef]
46. Zahedi Asl, V.; Zhao, J.; Anjum, M.J.; Wei, S.; Wang, W.; Zhao, Z. The effect of cerium cation on the microstructure and anti-corrosion performance of LDH conversion coatings on AZ31 magnesium alloy. *J. Alloys Compd.* **2020**, *821*, 153248. [CrossRef]